Journal of Power Sources 337 (2017) 65–72

Contents lists available at ScienceDirect

Journal of Power Sources

journal homepage: www.elsevier.com/locate/jpowsour

Electric double layer capacitors employing nitrogen and sulfur co-doped, hierarchically porous graphene electrodes with synergistically enhanced performance

Aravindaraj G. Kannan [a], Amaresh Samuthirapandian [b], Dong-Won Kim [a, *]

[a] Department of Chemical Engineering, Hanyang University, Seongdong-Gu, Seoul 04763, Republic of Korea
[b] Materials Science and Technology Division, Oak Ridge National Laboratory, Oak Ridge, TN 37831, United States

HIGHLIGHTS

- Nitrogen and sulfur co-doped, hierarchically porous graphene is synthesized.
- EDLC with co-doped graphene exhibits high capacitance and good cycling stability.
- Good performance is attributed to co-doping and hierarchical porous structures.

ARTICLE INFO

Article history:
Received 7 June 2016
Received in revised form
19 October 2016
Accepted 30 October 2016
Available online 9 November 2016

Keywords:
Graphene
Electric double layer capacitor
Co-doping
Cycle performance
Energy storage

ABSTRACT

Hierarchically porous graphene nanosheets co-doped with nitrogen and sulfur are synthesized via a simple hydrothermal method, followed by a pore activation step. Pore architectures are controlled by varying the ratio of chemical activation agents to graphene, and its influence on the capacitive performance is evaluated. The electric double layer capacitor (EDLC) assembled with optimized dual-doped graphene delivers a high specific capacitance of 146.6 F g^{-1} at a current density of 0.8 A g^{-1}, which is higher than that of cells with un-doped and single-heteroatom doped graphene. The EDLC with dual-doped graphene electrodes exhibits stable cycling performance with a capacitance retention of 94.5% after 25,000 cycles at a current density of 3.2 A g^{-1}. Such a good performance can be attributed to synergistic effects due to co-doping of the graphene nanosheets and the presence of hierarchical porous structures.

1. Introduction

Electrical double layer capacitors (EDLCs) have attracted considerable attention as preferential energy storage devices for hybrid electric vehicles and load leveling applications due to their high power densities and long cycle life [1,2]. EDLCs store electrical energy via non-Faradaic reactions in the double layer formed at the electrode and electrolyte interface, where no charges are transported across the interface [2]. Such a reaction mechanism is dependent on the surface characteristics of the electrode materials. Various carbon-based electrode materials have been widely explored for EDLC applications [3]. In particular, hierarchically porous activated carbon with controlled pore architectures have been actively investigated with regard to EDLCs [4,5]. The capacitive performance of these carbon materials is highly dependent on the carbon source and the type of activation process used to create the pores [6,7]. Graphene nanosheets with two-dimensional and sp^2-hybridized carbon structures have received tremendous attention for EDLC applications due to their high surface area, high electrical conductivity, chemical inertness, thermal stability and mechanical robustness [8–10]. The capacitive performance of EDLCs assembled with graphene-based electrode materials is dependent on various characteristics such as the surface area, number of graphene layers, pore size distribution and the presence of surface functional groups, which are primarily determined by the synthetic methods to prepare the graphene nanosheets [11]. Additionally, the capacitive performance of graphene-based EDLCs could be greatly enhanced by a rational design of active materials, electrode architectures and capacitor assemblies [12,13]. Recently, Kim et al. synthesized micron-scale graphene nanomeshes with

* Corresponding author.
E-mail address: dongwonkim@hanyang.ac.kr (D.-W. Kim).

http://dx.doi.org/10.1016/j.jpowsour.2016.10.109
0378-7753/

periodic nanoholes that exhibited superior capacitance performance [14]. In another instance, Liu et al. utilized the intrinsic surface capacitance of single-layer graphene by preparing curved graphene sheets to prevent their re-stacking during the synthetic process [15]. Apart from these strategies, heteroatom doping of graphene-based materials has been proved to be very effective in enhancing electronic conductivities and capacitive performance [16–19]. Several heteroatoms such as nitrogen, boron, sulfur, fluorine and phosphorus have been successfully doped into graphene nanosheets. Co-doping of graphene nanosheets with two or more heteroatoms has been shown to synergistically enhance performance through an increased asymmetry in charge and spin densities, in addition to the generation of induced structural distortions [20–22]. These characteristics result in enhanced electronic conductivity and easy adsorption of ions from the electrolyte to enhance the specific capacitance. In addition, the presence of doped heteroatoms improves the surface wettability of electrolyte, increases the number of active sites and facilitates electrostatic interactions with organic ions [23]. However, co-doping of graphene nanosheets along with engineered pore architectures has been rarely reported so far for EDLC applications [24–29].

In this study, hierarchically porous nitrogen and sulfur co-doped graphene nanosheets (m-NSG) with high surface area were synthesized using a simple hydrothermal method, followed by a pore activation step, as schematically illustrated in Fig. 1. Pore architectures were controlled by varying the amount of chemical activation agent in the second step, and its effect on the capacitive performance was investigated. EDLCs assembled with m-NSG electrodes exhibited high specific capacitance and stable cycling performance over 25,000 cycles in comparison to un-doped and single-heteroatom doped graphene electrodes.

2. Experimental

2.1. Synthesis of m-NSG

Graphite oxide was prepared from graphite powder (SP-1, 30 μm nominal particle size, Bay Carbon, USA) using a two-step modified Hummers' method. In the first step, graphite was pre-oxidized, as reported by Kovtyukhova et al. [30]. In subsequent step, further oxidation was carried out via Hummers' method [31]. The prepared graphite oxide was exfoliated using ultra-sonication to form graphene oxide (GO) nanosheets. The m-NSG preparation involved the synthesis of nitrogen and sulfur co-doped graphene nanosheets (NSG), followed by a pore activation step. NSG was prepared from GO and thiourea using a hydrothermal method as reported earlier [32], in which thiourea was used as a source for both dopants. In a typical synthesis procedure, GO (300 mg) was dispersed into 70 mL of DI water, followed by the addition of 900 mg of thiourea. The solution was stirred for 4 h prior to being transferred into a 100 mL Teflon-lined stainless steel autoclave, which was placed in a pre-heated oven at 180 °C. The autoclave was allowed to cool naturally, and the resulting NSGs were alternatively washed with DI water and ethanol, and were dried overnight in a vacuum oven at room temperature. NSG was activated using potassium hydroxide (KOH) as a chemical activation agent at 800 °C for 1 h in Ar atmosphere. NSG and KOH were mixed with different weight ratios (1:4, 1:5 and 1:6), and the resulting products were denoted as m-NSG(x), where x denotes the ratio of KOH to NSG. The powder was washed with a 10% hydrochloric acid solution to remove any metallic residues, followed by rinsing with excess DI water until the pH was neutralized. Finally, the obtained products were dried overnight in a vacuum oven at 120 °C. Single heteroatom (nitrogen or sulfur) doped (m-NG and m-SG) and un-doped (m-G) hierarchically porous graphene was also prepared using the same synthetic procedures used to obtain m-NSG with KOH/graphene ratio of 5 in the second step.

2.2. Electrode preparation and cell assembly

The electrodes were prepared by coating an ethanol-based slurry containing graphene-based active material, Ketjen black as a conductive carbon and Teflonized acetylene black binder (80:10:10 by weight) onto a stainless-steel mesh. The electrodes were dried in a vacuum oven at 160 °C for 4 h. To evaluate the cycling characteristics of the graphene-based electrodes, EDLCs were assembled by sandwiching a polypropylene separator (Celgard 3401) between two symmetrical graphene-based electrodes in a CR2032 cell. The cell was then injected with an electrolyte solution consisting of 1 M $LiPF_6$ in ethylene carbonate/dimethyl carbonate (1:1 by volume, battery grade, PANAX ETEC Co. Ltd). This electrolyte was chosen because it exhibited large electrochemical stability, and when used in EDLCs allowed an operative voltage of 3.0 V [14,33–35]. For performance comparison, the cell was also assembled with conventional liquid electrolyte (1 M tetraethyl ammonium tetrafluoroborate in acetonitrile, 1 M $TEABF_4$ in AN). The cell using commercialized activated carbon powder (MSP-20, Kansai Coke) was also assembled and investigated. All cells were assembled in an argon-filled glove box containing less than 1 ppm H_2O and O_2.

2.3. Characterization and measurements

Morphologies of the synthesized samples were examined with a scanning electron microscope (SEM, JEOL JSM-6300) and transmission electron microscopy (TEM, JEOL, JEM 2100F). Energy dispersive X-ray spectroscopy (EDS) mapping images were obtained to examine the distributions of heteroatoms in the m-NSG

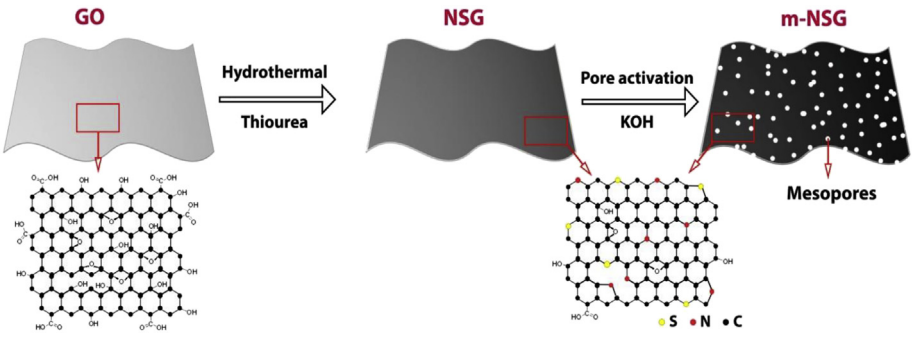

Fig. 1. Schematic illustration of the synthesis of m-NSG using a two-step method.

sample. The degree of doping and chemical composition of the graphene nanosheets were characterized using X-ray photoelectron spectroscopy (XPS, VG multilab ESCA system, 220i). Nitrogen adsorption/desorption isotherms were recorded after degassing the samples at 120 °C for 3 h using an Autosorb-IQ MP (Quantachrome INC.) apparatus at 77 K. Pore size distribution was obtained from an analysis of the adsorption branch of the isotherms using the Barret-Joyner-Halenda (BJH) method. Cyclic voltammetry was carried out using a Zahner Electrik IM6 potentiostat in the potential range of 0–3.0 V at various scan rates. Charge and discharge cycling testing of the cells was conducted at galvanostatic conditions over a voltage range of 0–3.0 V with battery testing equipment (WBCS 3000, Wonatech) at room temperature. Specific capacitance values of the cell were calculated, as reported earlier [36].

3. Results and discussion

The hierarchically porous and dual-doped graphene nanosheets were prepared from a two-step method, and the resulting product morphology was characterized using SEM measurements (Fig. 2). The SEM image of NSG (Fig. 2a) shows that a highly folded morphology formed after the hydrothermal step. The highly folded structure resulted from a large curvature created on the graphene surface as a result of the substitutional doping of carbon with larger-sized S heteroatoms [32]. Sheet-like and two-dimensional graphene structures were well preserved during the chemical activation step, as evident in Fig. 2b–d. All m-NSG(x) samples revealed a macroporous morphology, resulting from the difficulty in close packing of graphene nanosheets due to their highly folded morphology. When the KOH to graphene ratio was increased to 6, the m-NSG(6) sample showed a highly etched morphology with relatively large macropores. Single heteroatom doped graphenes (m-NG and m-SG) and un-doped graphene also exhibited a highly folded nanosheet morphology with macroporous structures, as shown in Fig. S1.

The morphology and distributions of doped heteroatoms were investigated using TEM and EDS elemental mappings, respectively. As expected, TEM image (Fig. 3a) of m-NSG(5) shows sheet-like morphology with highly porous structures. The elemental mappings of m-NSG(5) sample (Fig. 3b–f) show the overall distributions of carbon, oxygen, nitrogen and sulfur atoms throughout the sheet-like structures and the heteroatoms are present both on the basal plane and edges of m-NSG(5). This result confirms that the heteroatoms are successfully doped into the graphene nanosheets.

Influence with regard to the quantity of the activation agent on the pore architectures of m-NSG samples was evaluated using nitrogen adsorption/desorption isotherms, the results of which are given in Fig. 4. All m-NSG samples exhibited type IV isotherms with a sharp capillary condensation step and hysteresis loop, as depicted in Fig. 4a. The presence of a hysteresis loop indicated the existence of a large number of mesopores within the sample. As the KOH content increased, the magnitude of the hysteresis loop decreased. The BET surface area of m-NSG(4), m-NSG(5), and m-NSG(6) were measured to be 1161, 1278, and 1416 $m^2\ g^{-1}$, respectively, indicating that the specific surface area increased as the KOH content increased. The pore size distribution given in Fig. 4b revealed a wider pore size distribution for the m-NSG(4) sample with an average pore width of 4 nm, whereas the m-NSG(5) sample revealed a narrow size distribution of mesopores along with the presence of micropores. In contrast, m-NSG(6) mainly featured pores with pore diameter less than 2 nm. These results indicated that the m-NSG(6) sample predominantly showed micropores, while the other two samples featured a mixture of micro- and mesoporous structures. Based on the SEM images (Fig. 2) and nitrogen adsorption/desorption measurements (Fig. 4), we can conclude that the prepared m-NSG samples are hierarchically porous in nature with the presence of micro-, meso- and macropores. As a control sample, m-G also showed similar nitrogen adsorption/desorption isotherms and pore size distributions, as presented in Fig. S2, implying that the pore architecture

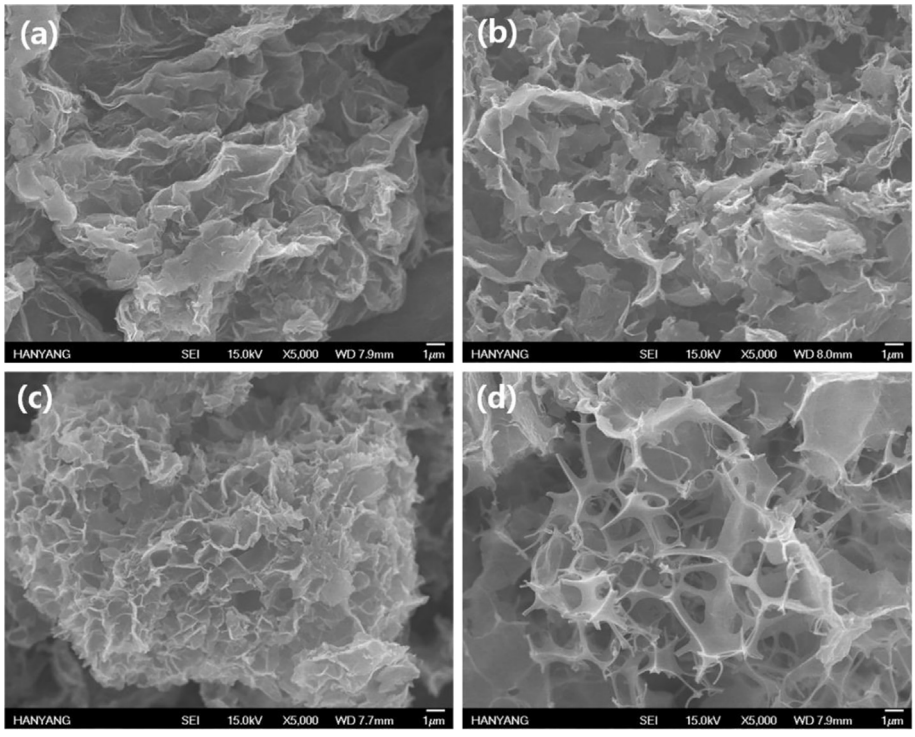

Fig. 2. SEM images of (a) NSG, (b) m-NSG(4), (c) m-NSG(5) and (d) m-NSG(6).

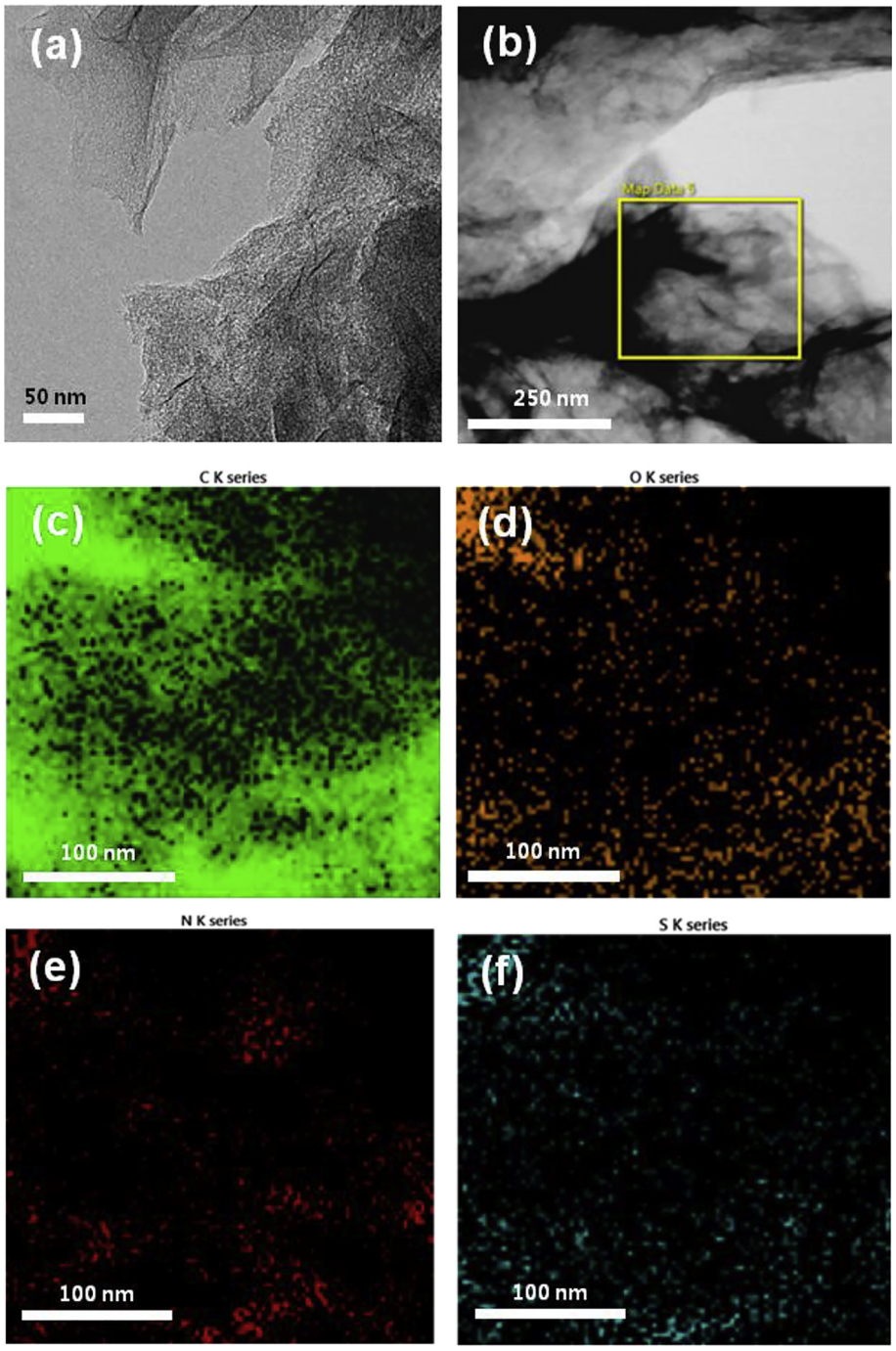

Fig. 3. (a) TEM image of m-NSG(5). (b) TEM image of m-NSG(5) and EDS elemental mappings corresponding to (c) carbon, (d) oxygen, (e) nitrogen and (f) sulfur.

was hardly affected by the doping of graphene nanosheets with dual-heteroatoms.

To confirm the doping of nitrogen and sulfur in the m-NSG sample, XPS was performed; the resultant survey spectra of the various graphene samples are given in Fig. 5. The survey spectrum of m-G revealed the presence of carbon and oxygen elements, whereas the survey spectrum of m-NSG(5) revealed the presence of carbon, oxygen, nitrogen and sulfur. This result confirmed the successful doping of dual-heteroatoms within the graphene nanosheets. The quantities of nitrogen and sulfur in m-NSG(5) were measured to be 1.49 and 2.16 at.%, respectively. The C/O ratio in m-G and m-NSG(5) was determined to be 12.6 and 11.3, respectively. A high C/O ratio in these samples indicated that the oxide functional groups on the GO surface were highly reduced during the hydrothermal method and thermal treatment during the pore activation step. In addition, thiourea could function as a reducing agent aside from its role as a dopant source [37].

The amounts of nitrogen and sulfur doping in m-NSG(4) sample (Fig. S3) were measured to be 1.53 and 2.12 at.%, respectively. In case of m-NSG(6), nitrogen and sulfur contents were found to be 1.46 and 2.18 at.%, respectively. These results suggest that the contents of doped heteroatoms are almost same irrespective of amount of pore activation agent. Since the N and S content in all three m-NSG(x) samples were found to be similar, its influence on

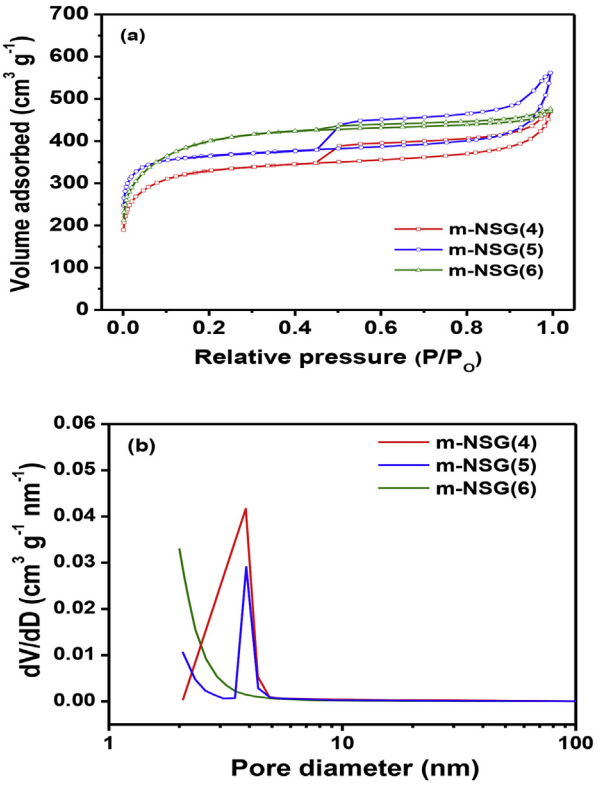

Fig. 4. (a) Nitrogen adsorption/desorption isotherms, and (b) pore size distributions of m-NSG samples activated with different quantities of KOH.

their capacitive behavior can be ignored in this study. In the case of single heteroatom doped samples, m-NG and m-SG revealed the presence of nitrogen and sulfur, respectively, along with the presence of carbon and oxygen. To understand the nature of doping, the high-resolution C 1s, N 1s and S 2p XPS spectra were resolved, and the results are given in Fig. 5 b–d. The C 1s peak could be resolved into three peaks centered at 284.5, 285.6 and 289.0 eV. The peak at 284.5 eV is attributed to sp^2-hybridized carbon and the peak at 285.6 eV can be ascribed to C–O, C–S and C–N groups [38]. The peak at 289.0 eV indicates the presence of residual carbonyl and carboxyl groups. The high-resolution N 1s peak was also resolved into three peaks, which correspond to pyridinic, pyrrolic and graphitic nitrogen [39]. The high-resolution S 2p peak given in Fig. 5d was resolved into two major peaks at 163.8 and 165.0 eV, which are attributed to sulfur atoms bound to aromatic carbon structures, indicating that sulfur was successfully doped into graphene nanosheets [40]. The other minor peak at higher binding energy is attributed to C-SO_x. These results demonstrate that sulfur and nitrogen atoms are bound to carbon framework in the m-NSG(5) sample.

The electrochemical performance of m-NSG(x) and m-G was evaluated by cyclic voltammetry in the potential range of 0–3.0 V. As depicted in Fig. 6a, the shape of the cyclic voltammograms (CVs) for all the samples was approximately rectangular and there were no redox reaction peaks, suggesting that charging and discharging were reversible at the electric double layer of the electrode. Although pseudocapacitance arising from functional groups could contribute slightly towards the overall capacitance, it could also degrade the cycling stability of the EDLC [41]. Based on this result, the present EDLC systems are expected to have better cycling stability than EDLCs with pseudocapacitance. Among all the tested

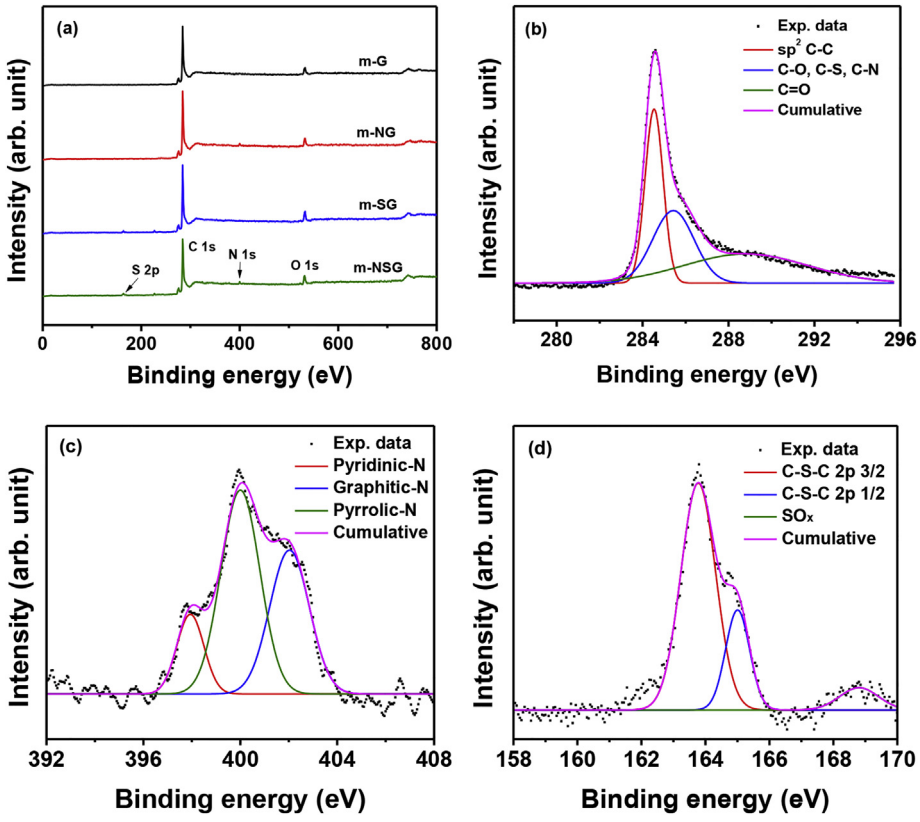

Fig. 5. (a) XPS survey spectra of m-NSG(5) and other control samples. High-resolution (b) C 1s, (c) N 1s and (d) S 2p XPS spectra of m-NSG(5) sample.

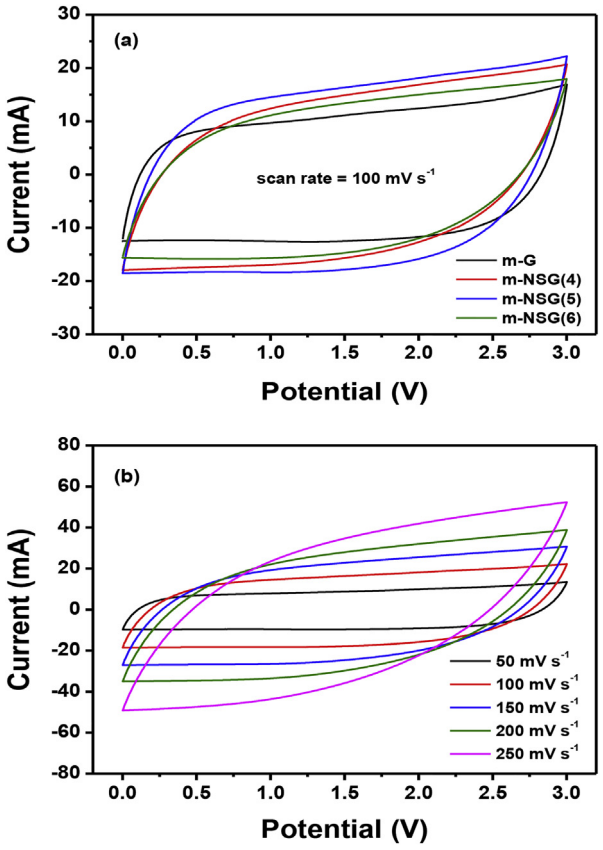

Fig. 6. (a) Cyclic voltammograms of EDLCs assembled with m-G and m-NSG(x) electrodes at a scan rate of 100 mV s^{-1}. (b) Cyclic voltammograms of an EDLC assembled with m-NSG(5) at different scan rates.

samples, m-NSG(5) exhibited the highest current response than the other materials. Moreover, even at higher scan rates, a rectangular shape was retained with little distortion, as shown in Fig. 6b. Good cycling performance at higher scan rates could be attributed to the hierarchical pore size arrangement in m-NSG(5), aiding ions to take a shortened path and adsorb ions easily over the pore surface through their pore network [42].

EDLCs assembled with m-NSG(x) were subjected to galvanostatic charge and discharge cycling between the voltage range of 0–3.0 V. The charge and discharge curves of EDLC with m-NSG(5) at different current rates were almost linear with time and were triangular in shape, as shown in Fig. 7a. These results confirmed its capacitive behavior and were well consistent with the CV results in Fig. 6. The EDLC assembled with m-NSG(5) delivered a high specific capacitance of 146.6 F g^{-1} at 0.8 A g^{-1}, which surpassed the performance of EDLC with activated carbon in the organic electrolyte. The graphene surface and its edge sites along with a large number of pores, can be the active sites for ionic adsorption. Herein, graphene activation prevented the graphene sheets from agglomerating and greatly increased the surface available for ion adsorption, resulting in a high specific capacitance. Fig. 7b presents the specific capacitance of the EDLCs assembled with m-NSG(x), which were obtained at different current rates. As expected, the capacitance of the cells decreased as the current rate increased. As shown in the figure, the cell with m-NSG(5) had the highest capacitance for all current rates. High capacitance of the m-NSG(5) was primarily attributed to its favorable pore size distribution rather than its surface area. As discussed earlier, m-NSG(5) possessed a combination of a high concentration of micropores and mesopores

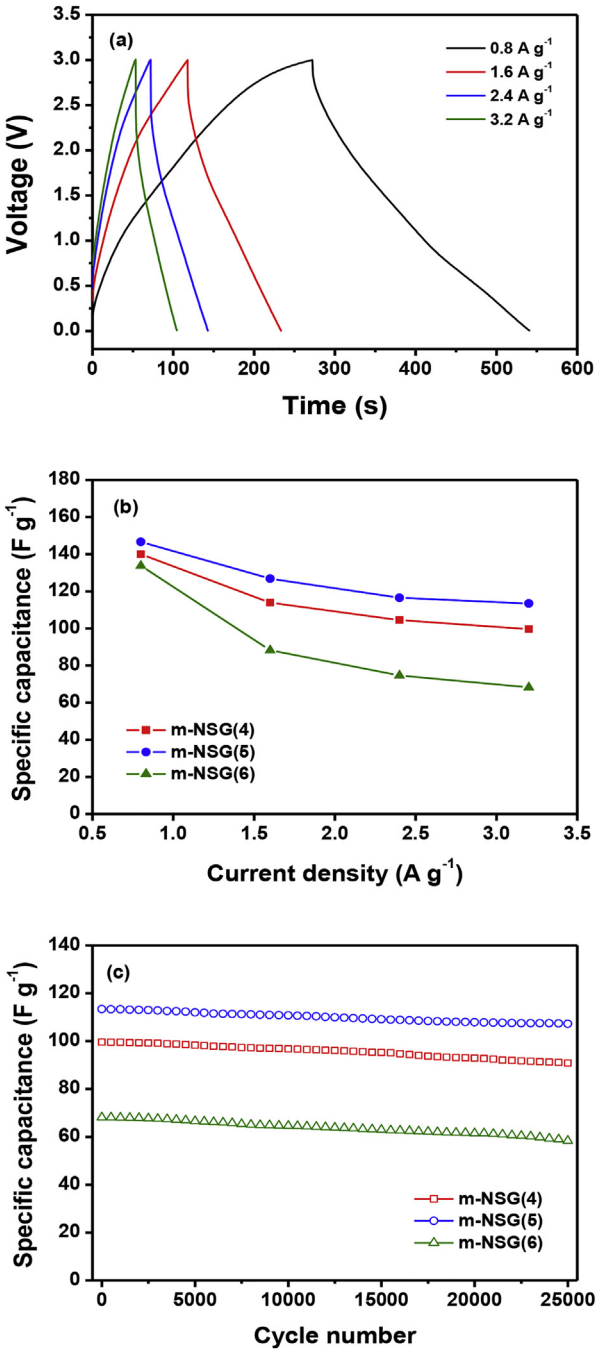

Fig. 7. (a) Charge and discharge curves of an EDLC with m-NSG(5) at different current rates. (b) Specific capacitance of EDLCs with m-NSG(x) as a function of the current rate. (c) Specific capacitance of EDLCs with m-NSG(x) as a function of the cycle number at a constant current rate of 3.2 A g^{-1}.

around 4.0 nm. In contrast, the cell with m-NSG(6) exhibited a poor rate performance, since the predominant presence of micropores may have slowed down the ionic diffusion and hindered the formation of an electric double layer. These results emphasized the necessity for electrode materials with micro- and mesopores for capacitance contribution in EDLC systems where organic electrolytes with large ionic radii are utilized [43]. Mesopores act as an electrolyte reservoir and provide ion-conducting channels, while micropores allow for easy ion accessibility, resulting in enhancement of the specific capacitance. Although, m-NSG(4) exhibits

hierarchical pore structures with the presence of macro, meso and micropores, the larger surface area of m-NSG(5) gives the better rate capability. The cycling stability of the EDLCs with m-NSG(x) electrodes was evaluated at a current rate of 3.2 A g^{-1}, and the results are presented in Fig. 7c. All cells exhibited excellent cycling stability over 25,000 cycles and low capacitance fading during cycling. In particular, the cell with m-NSG(5) exhibited good capacitance retention values of 94.5% after 25,000 cycles. The nitrogen and sulfur heteroatoms on the surface greatly enhanced the wettability of the electrode towards the electrolyte solution and helped achieve a greater utilization of the pores for the formation of an electric double layer. To demonstrate the reversible cycling behavior with an acceptable efficiency at high operating voltage, the coulombic efficiencies of the cells with m-NSG(5) were determined in different voltage ranges of 2.5, 2.7 and 3.0 V at a constant current density of 3.2 A g^{-1}. As shown in Fig. S4, the cells at all the tested voltages exhibited coulombic efficiency of >96%, indicating that the electrolyte ($LiPF_6$ in EC/DMC) used in this study was stable even at high voltage of 3.0 V.

Cycling performance of the EDLC with m-NSG(5) electrode was also evaluated using $TEABF_4$-AN as an electrolyte, and the results are given in Fig. S5. As shown in Fig. S5a, the cell using $TEABF_4$-AN showed the charge and discharge curves similar to the cell employing $LiPF_6$-EC/DMC at all the current rates. Fig. S5b presents the specific capacitance of the cells with different electrolytes. The cell with $TEABF_4$-AN electrolyte exhibited slightly higher capacitance than the cell using $LiPF_6$-EC/DMC at all the current rates. These results can be ascribed to higher ionic conductivity of $TEABF_4$-AN electrolyte (5.5×10^{-2} S cm^{-1}) as compared to that of $LiPF_6$-EC/DMC electrolyte (1.2×10^{-2} S cm^{-1}). With respect to cycling stability, the cell with $LiPF_6$-EC/DMC exhibited more stable capacitance retention (Fig. S5c), indicating that $LiPF_6$-EC/DMC electrolyte was more stable during cycling at high voltage (~3.0 V). In case of cell with AN-based electrolyte, the electrolyte decomposition at high voltage seemed to be the main cause for poor cycling stability of the cell [44].

The cycling stability of control samples (m-G, m-NG, m-SG) was investigated and compared with that of m-NSG(5) electrode (Fig. 8a). Un-doped graphene (m-G) exhibited an inferior cycling stability of 54.9% after 25,000 cycles with a low initial capacitance. Upon incorporating heteroatoms (N or S) into graphene, both specific capacitance and cycling stability were enhanced. Therefore, the incorporation of heteroatoms into graphene nanosheets could result in greater pore utilization by enhancing accessibility of the electrolyte within the pores, thereby increasing its capacitance. When nitrogen and sulfur heteroatoms were simultaneously incorporated into the graphene layers, the specific capacitance improved through facile electron transfer, and thus dual doping with N and S was an effective strategy toward improving the capacitive performance of the EDLC [16,24].

The influence of heteroatom doping on the rate capability was investigated by comparing the rate performance of m-NSG(5) with other control samples (Fig. 8b). As presented in the figure, the cell with the m-NSG(5) electrode exhibited the highest specific capacitance at all current rates. Since the electrodes were prepared using the same ratio of the activation agent to graphene, effects with regard to pore architectures on their rate capabilities could be neglected. The only possible factor to determine the rate performance of these electrodes was the presence of doped heteroatoms. Accordingly, these results substantiated that dual-heteroatom doping positively influenced the rate performance and cycling stability.

The electrochemical behavior of EDLC assembled with commercial activated carbon electrode is shown in Fig. S6, where its capacitance retention after 25,000 cycles is found to be 95.1%,

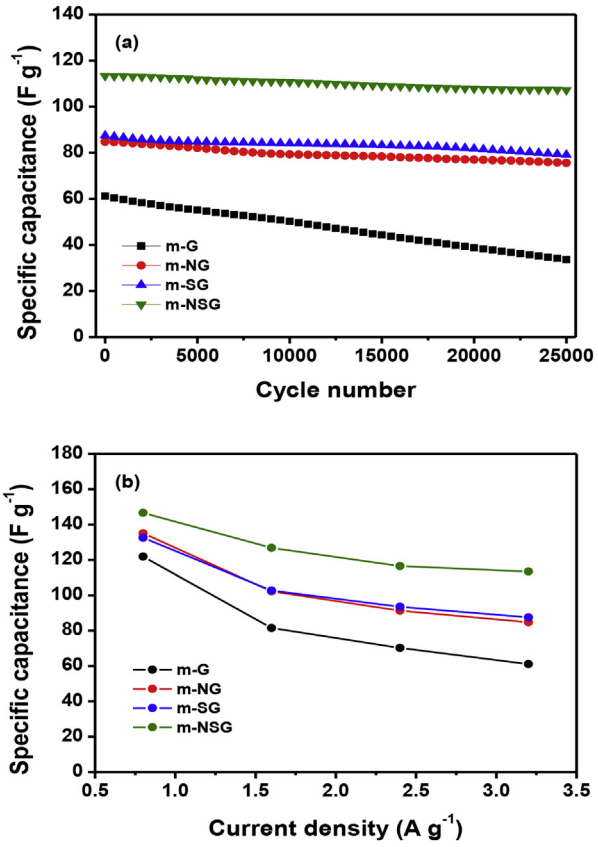

Fig. 8. (a) Specific capacitance of EDLCs with m-NSG(x) and control samples as a function of cycle number at 3.2 A g^{-1}, and (b) specific capacitance of EDLCs with m-NSG(x) and control samples as a function of the current rate.

which is similar to EDLC assembled with m-NSG(5) electrodes. However, EDLC assembled with commercial activated carbon electrode exhibited poor rate capability than the EDLC with m-NSG(5) electrode. This result demonstrates that the EDLC with m-NSG(5) has stable cycling performance comparable to commercial EDLCs and faster reaction kinetics. The superior performance of m-NSG(5) was primarily attributed to the following reasons: (i) an efficient utilization of graphene layers for surface adsorption by preventing their agglomeration during synthesis, (ii) favorable pore size distributions with a combination of micro- and mesopores formed by activation with KOH, (iii) activating graphene created more pores over the graphene surface, which further increased the area available for adsorption through the creation of a 3D architecture, and (iv) heteroatom co-doping greatly increased both the capacitance and stability by enhancing the electrical conductivity and electrolyte affinity of the material. These promising results offer new insight with regard to utilizing graphene in EDLCs to further improve their performance through activation techniques and dual heteroatom doping.

4. Conclusions

We demonstrated that the control of pore architectures and the dual-heteroatom doping of graphene nanosheets synergistically enhanced their specific capacitance and cycling stability. The improved performance of m-NSG(5) was attributed to the presence of a favorable combination of micro- and mesopores, helping the electrolyte to easily access the electrode surface. Dual-heteroatom doping also improved electrode wetting towards the electrolyte

solution, in addition to its electronic conductivity. As a result, the EDLC assembled with m-NSG(5) delivered a high specific capacitance of 146.6 F g^{-1} at a current density of 0.8 A g^{-1}, and exhibited stable cycling performance with a capacitance retention of 94.5% after 25,000 cycles at 3.2 A g^{-1}.

Acknowledgements

This work was supported by the Industrial Promotion Program of Economic Cooperation Area of MOTIE/KIAT [R0004005] and the National Research Foundation of Korea (NRF) grant funded by the Korea goverment (Ministry of Science, ICT and Future Planning) (No. 2016R1A4A1012224).

Appendix A. Supplementary data

Supplementary data related to this article can be found at http://dx.doi.org/10.1016/j.jpowsour.2016.10.109.

References

[1] N.-S. Choi, Z. Chen, S.A. Freunberger, X. Ji, Y.-K. Sun, K. Amine, G. Yushin, L.F. Nazar, J. Cho, P.G. Bruce, Angew. Chem. Int. Ed. 51 (2012) 9994–10024.
[2] R. Kotz, M. Carlen, Electrochim. Acta 45 (2000) 2483–2498.
[3] M. Inagaki, H. Konno, O. Tanaike, J. Power Sources 195 (2010) 7880–7903.
[4] E. Frackowiak, F. Beguin, Carbon 39 (2001) 937–950.
[5] J.-S.M. Lee, T.-H. Wu, B.M. Alston, M.E. Briggs, T. Hasell, C.-C. Hu, A.I. Cooper, J. Mater. Chem. A 4 (2016) 7665–7673.
[6] A.G. Pandolfo, A.F. Hollenkamp, J. Power Sources 157 (2006) 11–27.
[7] H.-H. Shen, C.-C. Hu, J. Electrochem. Soc. 161 (2014) A1828–A1835.
[8] M.D. Stoller, S. Park, Y. Zhu, J. An, R.S. Ruoff, Nano Lett. 8 (2008) 3498–3502.
[9] Y. Wang, Z. Shi, Y. Huang, Y. Ma, C. Wang, M. Chen, Y. Chen, J. Phys. Chem. C 113 (2009) 13103–13107.
[10] R.R. Salunkhe, Y.-H. Lee, K.-H. Chang, J.-M. Li, P. Simon, J. Tang, N.L. Torad, C.-C. Hu, Y. Yamauchi, Chem. Eur. J. 20 (2014) 13838–13852.
[11] L. Zhang, X. Yang, F. Zhang, G. Long, T. Zhang, K. Leng, Y. Zhang, Y. Huang, Y. Ma, M. Zhang, Y. Chen, J. Am. Chem. Soc. 135 (2013) 5921–5929.
[12] K. Chen, S. Song, F. Liu, D. Xue, Chem. Soc. Rev. 44 (2015) 6230–6257.
[13] Y. Zhu, S. Murali, M.D. Stoller, K.J. Ganesh, W. Cai, P.J. Ferreira, A. Pirkle, R.M. Wallace, K.A. Cychosz, M. Thommes, D. Su, E.A. Stach, R.S. Ruoff, Science 332 (2011) 1537–1541.
[14] H.-K. Kim, S.-M. Bak, S.W. Lee, M.-S. Kim, B. Park, S.C. Lee, Y.J. Choi, S.C. Jun, J.T. Han, K.-W. Nam, K.Y. Chung, J. Wang, J. Zhou, X.-Q. Yang, K.C. Roh, K.-B. Kim, Energy Environ. Sci. 9 (2016) 1270–1281.
[15] C. Liu, Z. Yu, D. Neff, A. Zhamu, B.Z. Jang, Nano Lett. 10 (2010) 4863–4868.
[16] X. Wang, G. Sun, P. Routh, D.-H. Kim, W. Huang, P. Chen, Chem. Soc. Rev. 43 (2014) 7067–7098.
[17] W. Yang, M. Ni, X. Ren, Y. Tian, N. Li, Y. Su, X. Zhang, Curr. Opin. Colloid In. 20 (2015) 416–428.
[18] Z. Li, B. Li, Z. Liu, D. Li, H. Wang, Q. Li, Electrochim. Acta 190 (2016) 378–387.
[19] Y. Li, S. Zhang, H. Song, X. Chen, J. Zhou, S. Hong, Electrochim. Acta 180 (2015) 879–886.
[20] J.P. Paraknowitsch, A. Thomas, Energy Environ. Sci. 6 (2013) 2839–2855.
[21] J.-H. Kim, A.G. Kannan, H.-S. Woo, D.-G. Jin, W. Kim, K. Ryu, D.-W. Kim, J. Mater. Chem. A 3 (2015) 18456–18465.
[22] U.B. Nasini, V.G. Bairi, S.K. Ramasahayam, S.E. Bourdo, T. Viswanathan, A.U. Shaikh, J. Power Sources 250 (2014) 257–265.
[23] S.-M. Li, S.-Y. Yang, Y.-S. Wang, H.-P. Tsai, H.-W. Tien, S.-T. Hsiao, W.-H. Liao, C.-L. Chang, C.-C.M. Ma, C.-C. Hu, J. Power Sources 278 (2015) 218–229.
[24] T. Akhter, M.M. Islam, S.N. Faisal, E. Haque, A.I. Minett, H.K. Liu, K. Konstantinov, S.X. Dou, ACS Appl. Mater. Inter. 8 (2016) 2078–2087.
[25] Z.-S. Wu, A. Winter, L. Chen, Y. Sun, A. Turchanin, X. Feng, K. Mullen, Adv. Mater. 24 (2012) 5130–5135.
[26] X. Yu, Y. Kang, H.S. Park, Carbon 101 (2016) 49–56.
[27] Y. Wen, T.E. Rufford, D. Hulicova-Jurcakova, L. Wang, ChemSusChem 9 (2016) 513–520.
[28] T. Wang, L.-X. Wang, D.-L. Wu, W. Xia, D.-Z. Jia, Sci. Rep. 5 (2015) 9591.
[29] V.G. Bairi, U.B. Nasini, S. Kumar Ramasahayam, S.E. Bourdo, T. Viswanathan, Electrochim. Acta 182 (2015) 987–994.
[30] N.I. Kovtyukhova, P.J. Ollivier, B.R. Martin, T.E. Mallouk, S.A. Chizhik, E.V. Buzaneva, A.D. Gorchinskiy, Chem. Mater. 11 (1999) 771–778.
[31] W.S. Hummers, R.E. Offeman, J. Am, Chem. Soc. 80 (1958), 1339–1339.
[32] A.G. Kannan, J. Zhao, S.G. Jo, Y.S. Kang, D.-W. Kim, J. Mater. Chem. A 2 (2014) 12232–12239.
[33] W. Li, D. Chen, Z. Li, Y. Shi, Y. Wan, G. Wang, Z. Jiang, D. Zhao, Carbon 45 (2007) 1757–1763.
[34] A. Laheaar, A. Janes, E. Lust, J. Electroanal. Chem. 669 (2012) 67–72.
[35] F. Beguin, V. Presser, A. Balducci, E. Frackowiak, Adv. Mater. 26 (2014) 2219–2251.
[36] K. Karthikeyan, S. Amaresh, S.N. Lee, X. Sun, V. Aravindan, Y.-G. Lee, Y.S. Lee, ChemSusChem 7 (2014) 1435–1442.
[37] C.K. Chua, A. Ambrosi, M. Pumera, J. Mater. Chem. 22 (2012) 11054–11061.
[38] Y. Dong, H. Pang, H.B. Yang, C. Guo, J. Shao, Y. Chi, C.M. Li, T. Yu, Angew. Chem. Int. Ed. 52 (2013) 7800–7804.
[39] Y. Chang, F. Hong, C. He, Q. Zhang, J. Liu, Adv. Mater 25 (2013) 4794–4799.
[40] Z. Yang, Z. Yao, G. Li, G. Fang, H. Nie, Z. Liu, X. Zhou, X.A. Chen, S. Huang, ACS Nano 6 (2011) 205–211.
[41] P. Azais, L. Duclaux, P. Florian, D. Massiot, M.-A. Lillo-Rodenas, A. Linares-Solano, J.-P. Peres, C. Jehoulet, F. Beguin, J. Power Sources 171 (2007) 1046–1053.
[42] D. Lozano-Castello, D. Cazorla-Amoros, A. Linares-Solano, S. Shiraishi, H. Kurihara, A. Oya, Carbon 41 (2003) 1765–1775.
[43] G. Salitra, A. Soffer, L. Eliad, Y. Cohen, D. Aurbach, J. Electrochem. Soc. 147 (2000) 2486–2493.
[44] P.W. Ruch, D. Cericola, A. Foelske, R. Kotz, A. Wokaun, Electrochim. Acta 55 (2010) 2352–2357.